Lab on a Chip

Special Issue on Circulating Tumor Cells

Title:

Isolation and mutational analysis of circulating tumor cells from lung cancer patients with magnetic sifters and biochips.

ELECTRONIC SUPPLEMENTARY INFORMATION

Christopher M. Earhart[a], Casey E. Hughes[b], Richard S. Gaster[c], Chin Chun Ooi[d], Robert J. Wilson[a], Lisa Y. Zhou[e], Eric W. Humke[b], Lingyun Xu[f] , Dawson J. Wong[g], Stephen B. Willingham[h], Erich J. Schwartz[i], Irving L. Weissman[h,i], Stefanie S. Jeffrey[j], Joel W. Neal[b,e], Rajat Rohatgi[b], Heather A. Wakelee[b,e], Shan X. Wang*[a,g,k]

[a]*Department of Materials Science and Engineering, Stanford University, Stanford, CA 94305, USA.*
[b] *Division of Oncology, Department of Medicine, Stanford University School of Medicine, Stanford, California 94305, USA.*
[c]*Department of Bioengineering, Stanford University, Stanford, CA 94305, USA.*
[d]*Department of Chemical Engineering, Stanford University, Stanford, CA 94305, USA.*
[e]*Stanford Cancer Institute, Stanford, CA 94305, USA.*
[f]*Department of Radiology, Stanford University, Stanford, CA 94305, USA.*
[g]*Department of Electrical Engineering, Stanford University, California 94305, USA*
[h]*Institute for Stem Cell Biology and Regenerative Medicine and the Ludwig Cancer Center, Stanford, CA 94305, USA.*
[i]*Department of Pathology, Stanford University School of Medicine, Stanford, CA 94305, USA.*
[j]*Department of Surgery, Stanford University, Stanford, CA 94305, USA.*
[k]*Geballe Laboratory for Advanced Materials, Stanford University, McCullough Building, Room 351, 476 Lomita Mall, Stanford, CA, 94305-4045. E-mail: sxwang@stanford.edu; Tel: +1 650-723-8671*

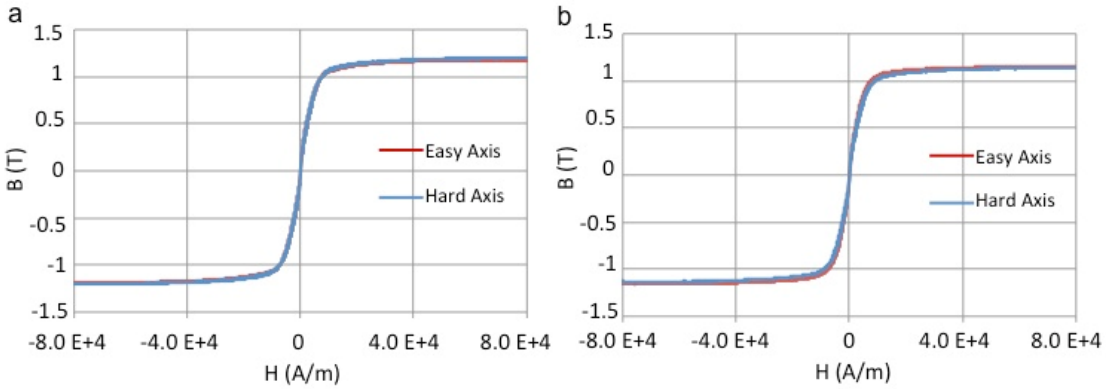

Supplementary Fig. 1 Magnetic sifter magnetic film properties. (**a**) B-H loop of the sifter die following deposition of a 12 micron thick permalloy ($Ni_{80}Fe_{20}$) film, exhibiting soft magnetic behavior. (**b**) B-H loop of same magnetic sifter after 4 weeks of storage in PBS and experimental use. No degradation of magnetic film properties was observed.

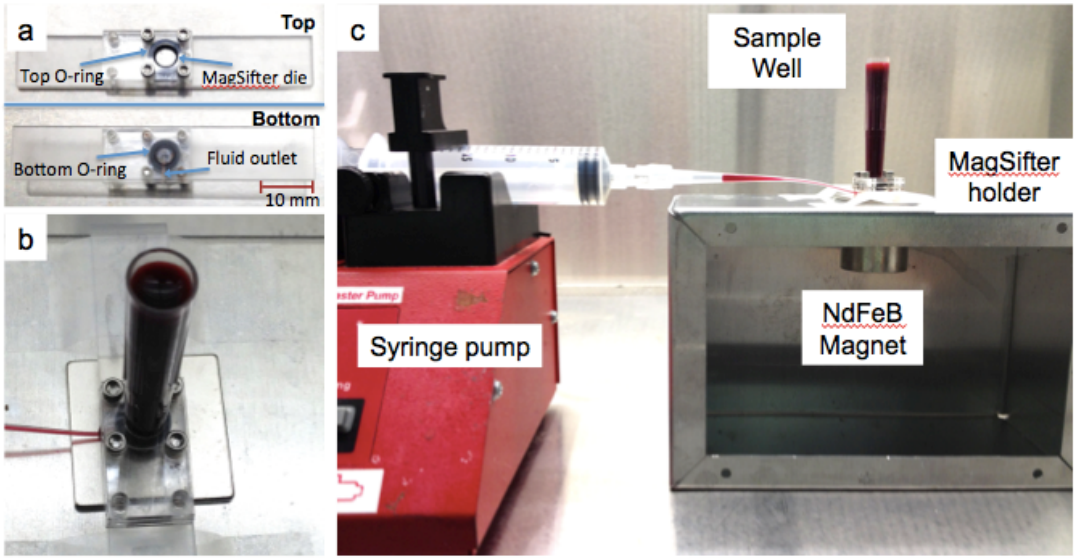

Supplementary Fig. 2 Experimental apparatus. (**a**) The magnetic sifter die is secured in an acrylic holder with O-rings to create a fluid tight seal around the patterned pore area. (**b**) Blood samples are loaded into a well situated above the magnetic sifter and pulled through into a fluid outlet underneath. (**c**) The magnetic sifter holder is positioned above a neodymium-iron-boron magnet during the capture step, and the blood sample is pulled through the magnetic sifter with a programmable syringe pump.

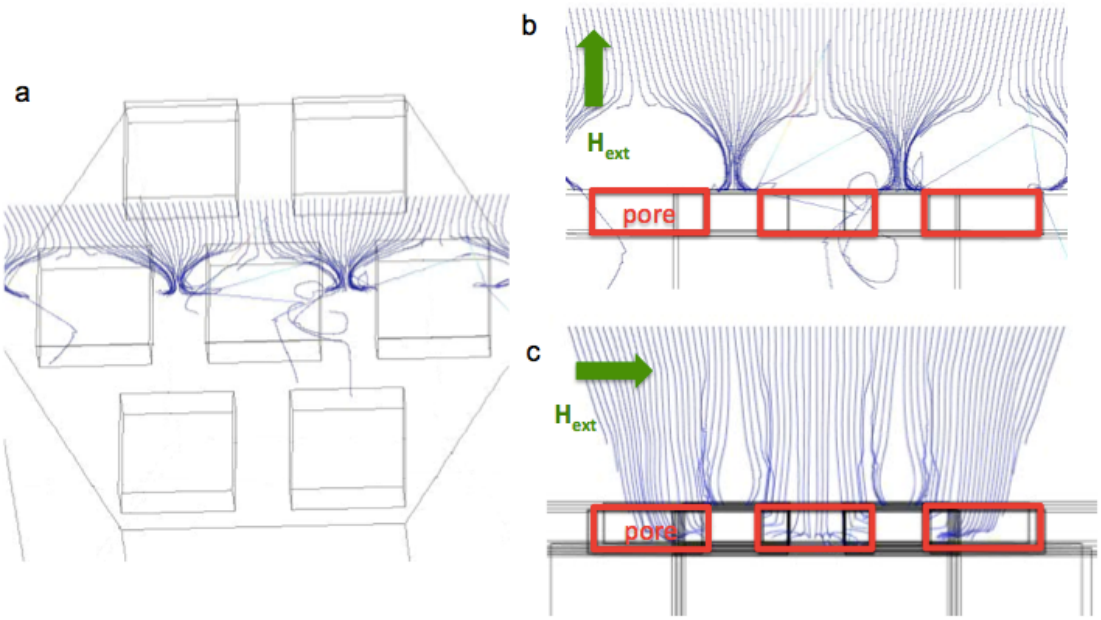

Supplementary Fig. 3 Simulation results. Simulation geometry and calculated trajectories of magnetically labeled cells. (**a**) Top-view, perpendicular external field. (**b**) Cross-section view of the center three pores for perpendicular external field configuration. Magnetically labeled cells move towards the edges of the pore due to the high local field gradients. (**c**) Corresponding trajectories for a parallel external magnetizing field. Magnetically labeled cells move towards the sides of the pore as they pass through the array.

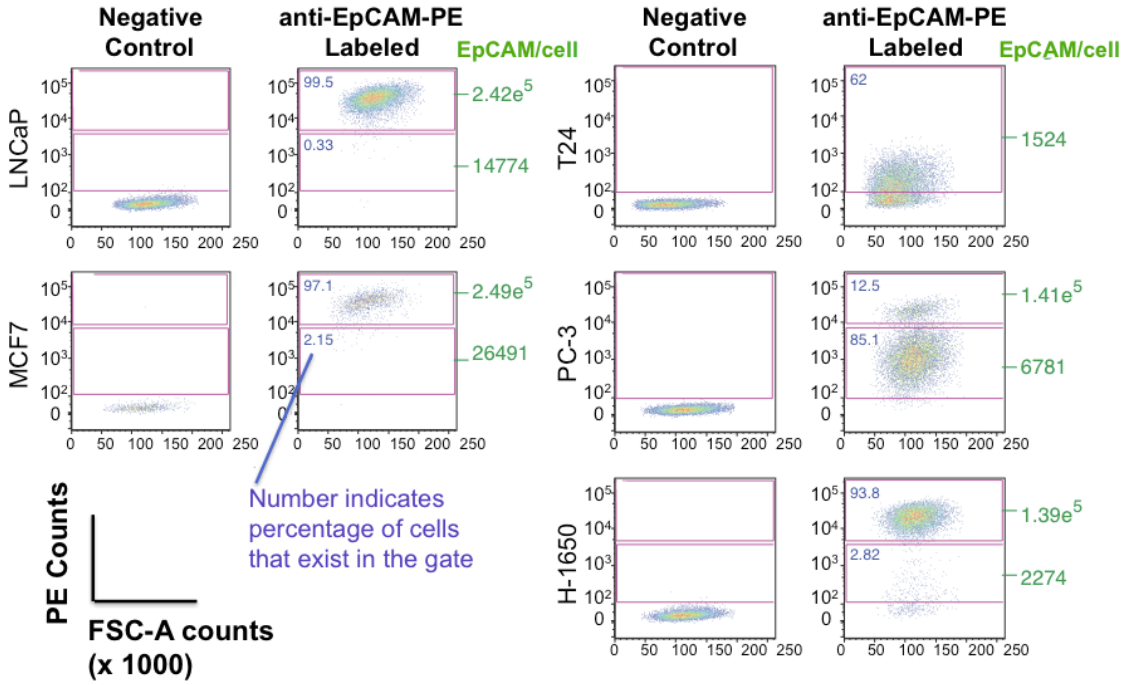

Supplementary Fig. 4 Quantification of cellular EpCAM. Scatter plots of phycoerythrin (PE) fluorescence intensity versus forward scatter intensity for various cell lines used in spiking experiments with the magnetic sifter. Median absolute EpCAM antibody binding sites for each cell line was determined from a calibration curve constructed from measurements on QuantiBRITE PE beads.

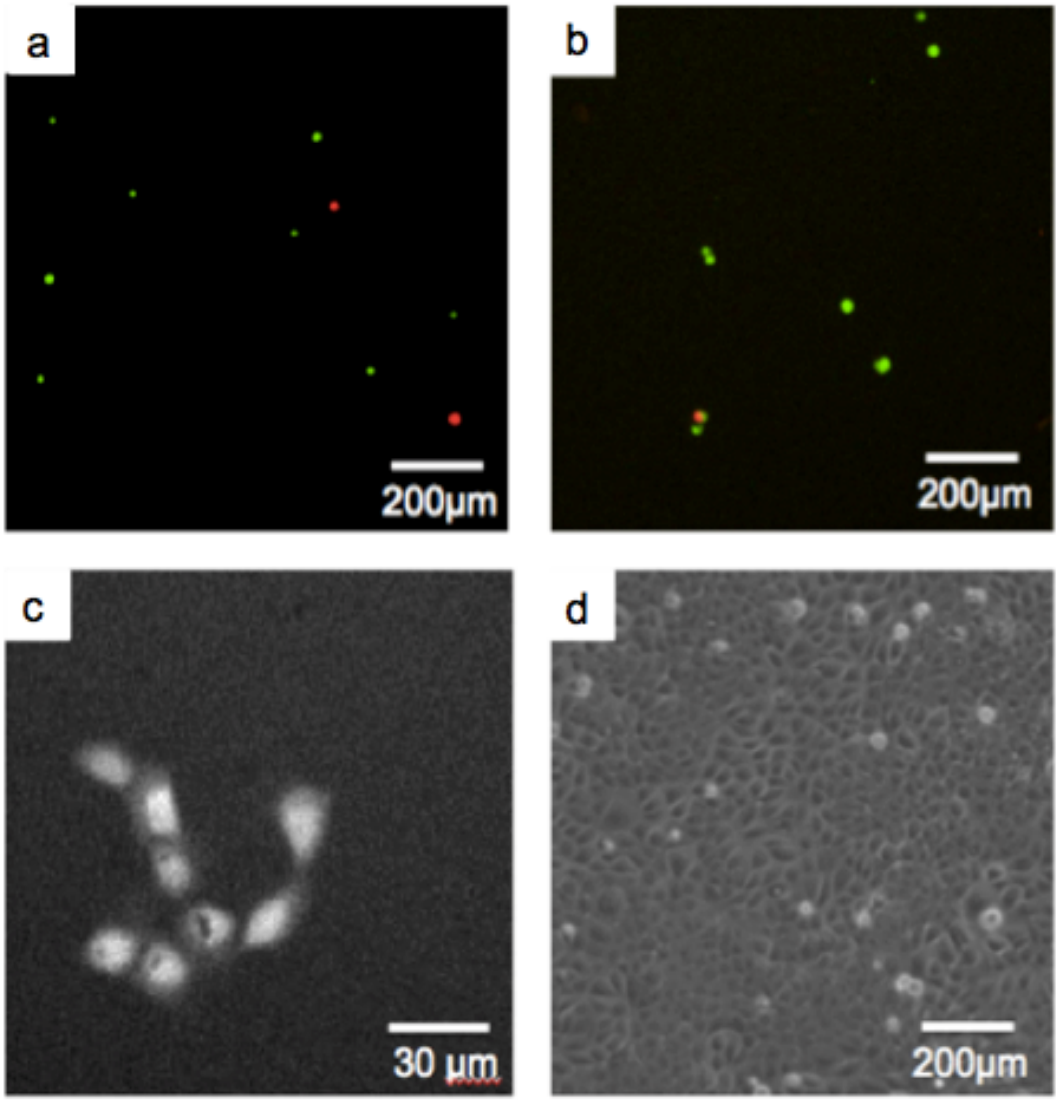

Supplementary Fig. 5 Cell viability and reculturing. H-1650 cells were stained with a LIVE/DEAD viability kit (Invitrogen, Cat.#L-3224) before (**a**) and after (**b**) magnetic labeling and processing with the magnetic sifter. Live cells fluoresce green, whereas dead cells fluoresce red. The ratio of live to dead cells was observed to remain unchanged after separation with the magnetic sifter. H-1650 cells, prelabeled with green CellTracker dye, were also spiked into whole blood, separated with the magnetic sifter and eluted into a 64-well plate for cell culture. Cells were eluted in media (see Materials and Methods) and maintained in an incubator at 37^{o}C in 5% CO_2. (**c**) A fluorescence micrograph of a cluster of H-1650 cells four days after processing with the magnetic sifter. (**d**) A bright-field optical micrograph of a confluent well three weeks after processing with the magnetic sifter.

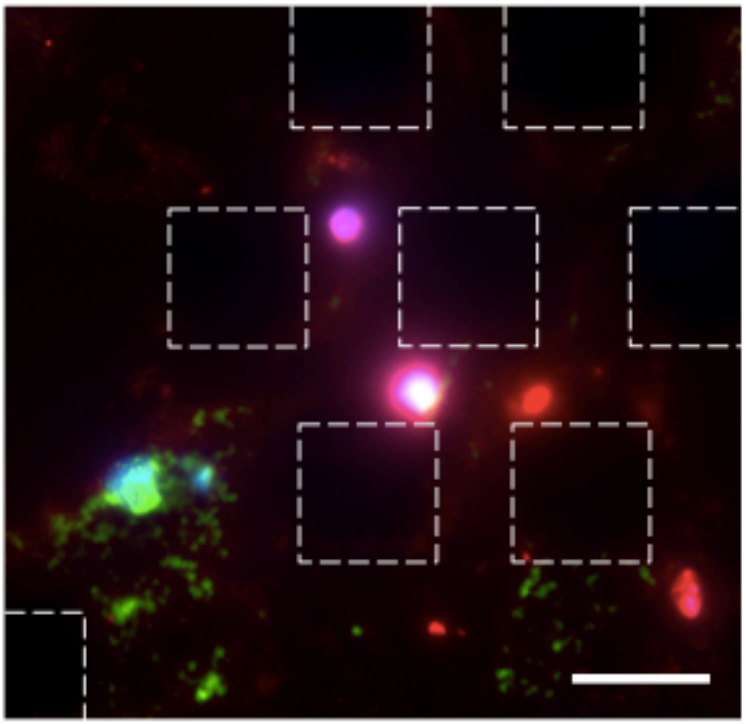

Supplementary Fig. 6 Cell scored as CTC from healthy donor sample. Merged fluorescence image (DAPI (blue), CD-45-PE (red), CK-FITC (green)) containing a cell captured from a healthy donor blood sample and scored as a CTC. The magnetic sifter pores are outlined by dashed boxes. Scale bar is 40 μm.

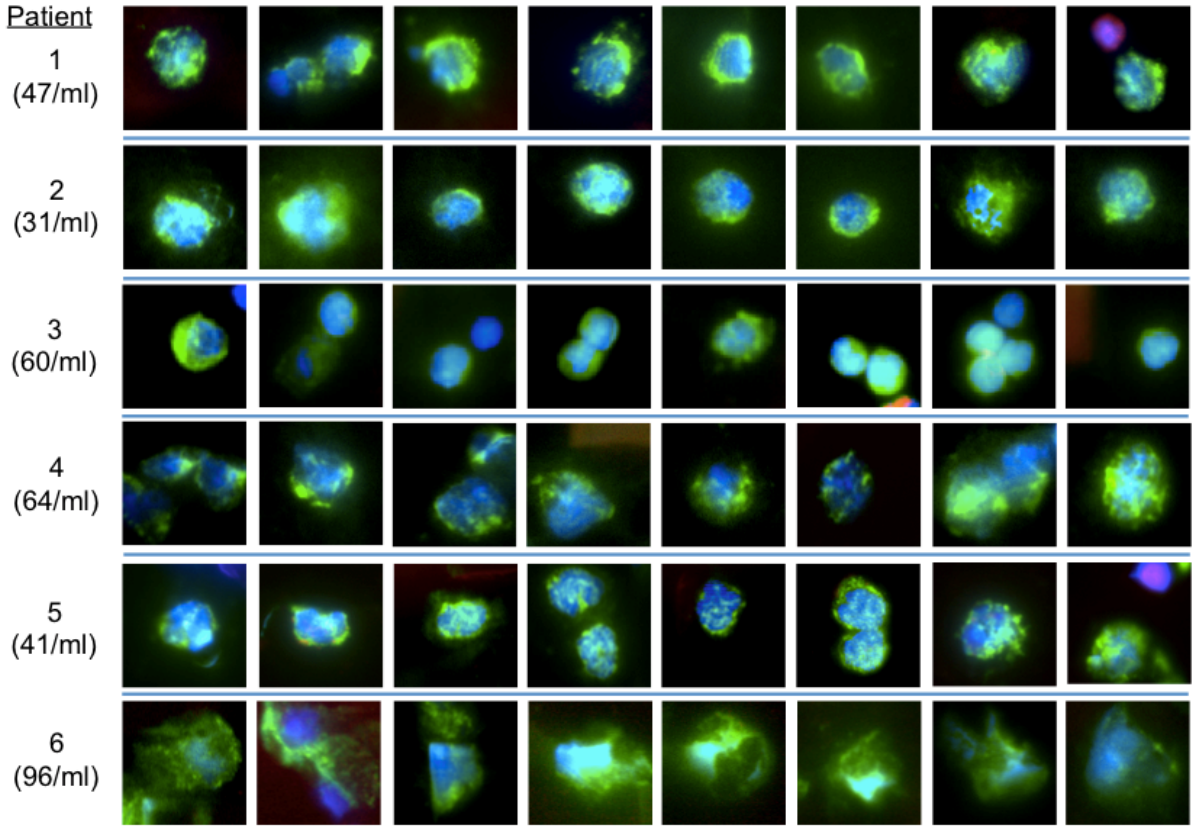

Supplementary Fig. 7 Cell image galleries. Examples of cells scored as circulating tumor cells from patient samples enumerated in this work. Each tile is 30 μm x 30 μm.

Operation in Lateral Flow Configuration - Supplementary Movies

Separations can be performed in either the vertical flow mode described throughout, or in a "lateral flow" configuration which allows real time optical characterization. In the lateral mode, the pore array is housed between 2 transparent windows which are spaced 100 μm above and below the porated, 500 μm thick, wafer which supports the magnetic film. The 100 μm gaps are chosen to be thin enough to provide adequate optical transmission for optical imaging through strongly absorbing whole blood samples, while millimeter gaps can be used for sufficiently dilute cell suspensions. In our upright microscope, the flow cell is usually oriented so that the magnetic film is on top and suspended cells flow through a slot at the edge and just above the pore array. Reflected white light is used for bright field imaging of the magnetic film surface and of cells suspended above it, and a mercury lamp provides fluorescence excitation from above. The flow cell can be inverted on the microscope stage to provide images of the silicon web on the die backside, which provides a view of cells exiting the pore array. Backlighting, with weak white light illumination from below the pore array, is useful for identifying pore locations in fluorescence mode, but the relatively long optical path length, through the 0.5 mm thick wafer

and abutting 100 μm gaps, causes strong optical absorption for light which is transmitted through the pores when the pores are filled with whole blood. A drain hole, located beneath and at the radial center of the pore array, collects cells and fluid which have flowed through the pores. For imaging the full area of the pore array in Supplementary Movies 1 and 2, we used a 2.5x objective with a small numerical aperture (NA) of 0.07, which produces images with resolution and pixel spacing near 10 μm and a depth of field of about 100 μm. Thus cells are not sharply focused, but the focus is maintained over the entire 100 μm gap between magnetic film and window. Illumination is spread over a 5mm area, so fluorescence excitation, and hence emission, is quite weak compared to higher magnification images.

We have used this configuration to record images during flow of blood/PBS samples, spiked with H1650 cells dyed with CellTracker™ green, at various flow rates and for selected PBS/Blood dilutions. Supplementary Movie 1 shows image streams for a 1:1 PBS:blood mixture which is flowed at ~ 1 mL hr^{-1} flow rate. Supplementary Figure 8 includes selected images from this movie. At very low flow rates, < 1 mL hr^{-1}, much of the initial fluid (PBS) within the flow cell remains stationary and the injected fluid flows in a relatively narrow region that is roughly directed towards the central drain hole. In this case, the flow patterns may assume some laminar flow characteristics near the narrow feed and drain ports, but laminar flow within in the flow cell body is not well developed**.** As the flow rate increases to 1 mL hr^{-1}, the input flow, which emanates from the feed slot that is fed by a tube that runs in the "up" direction (arrow in Supplementary Figure 8a), flows toward the central drain hole while extending into the central and upper right portion of the pore array due to inertial effects from the feed flow. The Reynolds number, using aqueous density and viscosity and a 1 mm sec^{-1} velocity, is about equal to the scale length (in mm), so strong turbulence is not expected. In ideal circumstances, we would expect the blood sample to provide uniform optical absorption in the regions which it fills, but this is often not observed at low flow rates. Instead, it is found that the blood sample does darken the reflected images, but this darkening can appear in narrow "stripes" (separated by transparent regions at the lower left). Because the darkness of regions corresponds to the local red blood cell density, due to their strong optical absorption, and because the flow patterns are smooth and continuous, the transparent "striped" regions between the dark stripes must be comprised of flowing transparent fluid. The cells that would be expected to flow within these transparent stripes have been accumulated or deflected into the adjacent dark stripes, where the cell concentration is thus significantly increased over that of the feed suspension. In the upper right of this image, a large region is observed to progressively become more opaque than the initial diluted blood sample, again implying that the local density of blood cells has increased beyond the density of the feed suspension. This highly darkened region must have high cell densities, but not necessarily a high local cellular flow rate. These cellular flow rates are best determined from cell trajectories observed using fluorescence, as described below, and such analysis reveals no mobile cells in this region, implying that this dark region is actually a blockage to cell flow. Such blockages can initially arise when clumps of cells restrict cell flow, but continue to allow fluid flow to deliver more cells to the clump. In addition to such clumping effects, the effective local viscosity can also significantly increase, due to the high local volume fraction of cells, which further reduces both cell and fluid flow. This can ultimately lead to an instability where flow of both cells and fluid becomes obstructed, resulting in local "clogging". To track actual cell flow we spiked H1650 lung cancer tumor cells, dyed with CellTracker green, into PBS/blood mixtures and recorded video images of fluorescence during flow. A multiply

exposed fluorescence image is shown in Supplementary Figure 8b. The trajectories of spiked cells, regional cell velocity variations, "striped" flow regions where cells are deflected out of transparent regions and into dark regions due to cell flow blockages in the input slot, and of gross blockages (dark regions where no fluorescent cells move) on the magnetic sifter surface (arrow) are apparent. Similar effects in simple lateral flow cells have been described previously, and are also associated with flows which have inadequate shear to disrupt cell-cell or cell-surface interactions or to disrupt cell complexes by deforming cell shapes.

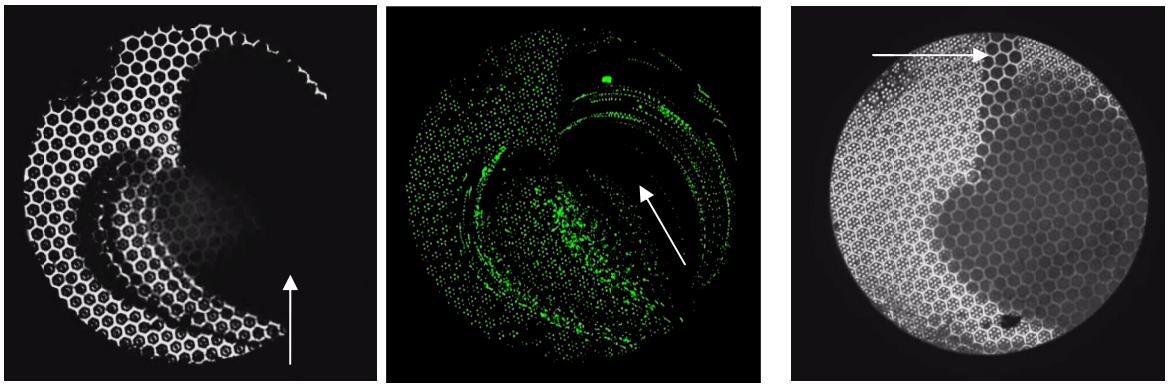

(a) (b) (c)

Supplementary Fig. 8 (**a**). Reflected light image of diluted blood sample (PBS:blood = 1:1) flowing into lateral flow cell at 1 mL hr^{-1}. Dark regions correspond to the presence of absorbing red blood cells. The inlet tube is along the arrow, and the pore array diameter is 5 mm. (**b**) Multiply exposed image showing trajectories of spiked fluorescent cells, with pores visualized by backlighting the pore array. Note many cells flowing in "stripes" (lower left) which appear dark in (**a**), while a large region near center right appears to obstruct cell flow (arrow). Variations in cell velocities are evident from the spacing of dots (cells) along trajectories in this image. (**c**) More dilute samples (PBS:blood = 4:1) are more transparent and flow more easily, so no densification is observed at this flow rate. Flow through the central drain hole outlet leads to darkening in the exit tube (arrow) which is made visible by including backlighting.

These effects can be avoided by further dilution of the initial samples, which reduces the opacity and effective viscosity and diminishes the probability of cell aggregate formation, as shown in Supplementary Figure 8c. Unfortunately, dilution seriously compromises blood throughput.

Problems with aggregate formation can also be eliminated by operating at higher flow rates as shown in Supplementary Movie 2. Supplementary Figure 9a shows an excerpted reflected light image as a sample (PBS/blood = 1/1) is flowed at 10 mL hr^{-1} and begins to fill the flow cell. Here the laminar flow character within the flow cell is much better developed, as the flow is now symmetrical with respect to the inlet/outlet axis. Supplementary Figure 9b shows multiply exposed trajectories of dyed H1650 cells, which now appear as streaks because of the increased flow rate, superimposed on a reflected light image which shows the blood sample filled regions of the flow cell when the flow reaches steady state. The direct visualization of fluorescently labeled CTC in flow indicates possibilities for flow cytometry identification of CTC, although the fluorescence of typical CTC stains is much weaker than that of CellTracker staining. Supplementary Figure 9c shows a reflected light image when the blood sample is nearly exhausted and the feed lines contain PBS. The last vestiges of the sample appear at various

localized regions of the input slot and flow along smooth paths which are consistent with the fluorescent cell trajectories, negligibly affected by diffusion or the aggregation induced flow obstructions observed at lower flow rates.

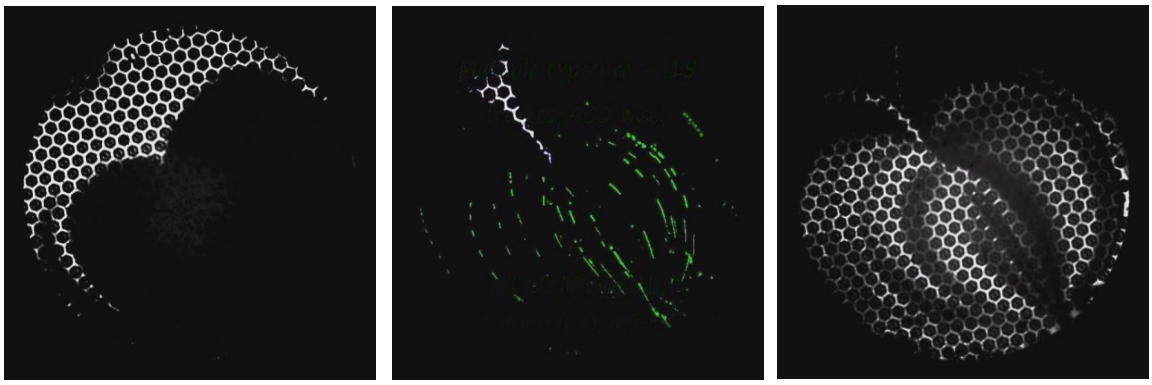

(a) (b) (c)

Supplementary Fig. 9 (**a**) Reflected light image of blood/PBS mixture (PBS:blood = 1:1) as flow at 10 mL hr^{-1} has partially filled the flow cell. At this flow rate, the laminar flow character within the flow cell is well developed and the stripes and blockages of Supplementary Figure 8b are absent. (**b**) The flow gradually fills the flow cell nearly completely at steady state, and the superimposed fluorescent H1650 trajectories illustrate the expected radial decay character of cell velocities, which are thus highly non-uniform over the pore array. At this flow rate cells near the inlet appear as streaks with lengths which correspond to mm sec^{-1} cell velocities, while cells near edges travel much more slowly. (**c**) When the blood sample is nearly consumed, the cell inflow becomes localized to various points in the entry slot. A reflected light image shows the location of the flow paths associated with different entry points, showing that cells move on very specific paths in steady state.

An examination of the cell velocities in different locations, from either streak length or spacing along fluorescent trajectories, reveals a large spatial heterogeneity in cell velocities, so that spatial variations in magnetic trapping efficiencies must be anticipated for this configuration. This is highly undesirable when attempting to extend magnetic capture to weaker magnetic labeling by lowering flow rates; suggesting a need to avoid the long range parabolic velocity profiles of laminar flow in simple lateral flow cells.

To uniformize the macroscopic variations of flow velocities, we therefore choose a vertical flow configuration. Here the sample is fed through a large diameter tube placed directly above the pore array. Because the pore array obstructs flow over most of its area, the flow transforms from the characteristic parabolic velocity distribution of the tube, where velocity ~ $1- r^2/R^2$ with r the radial coordinate and R the tube radius at large distances from the pore array, and becomes more uniform as z approaches the sifter surface. Flow velocities through the pores thus become quite homogenous over the sifter area, similar to the uniformity of flow among individual nozzles in a shower head. For more quantitative insight, a COMSOL simulation has been performed to show the fluid velocity variations across the surface of a pore array, which is displayed in Supplementary Figure 10. Clearly the difference in flow velocities between pores located at the

pore array center and edge is greatly reduced (about 10% variation) as compared to the large radial variation ($1- r^2/R^2$) expected for unimpeded laminar flow.

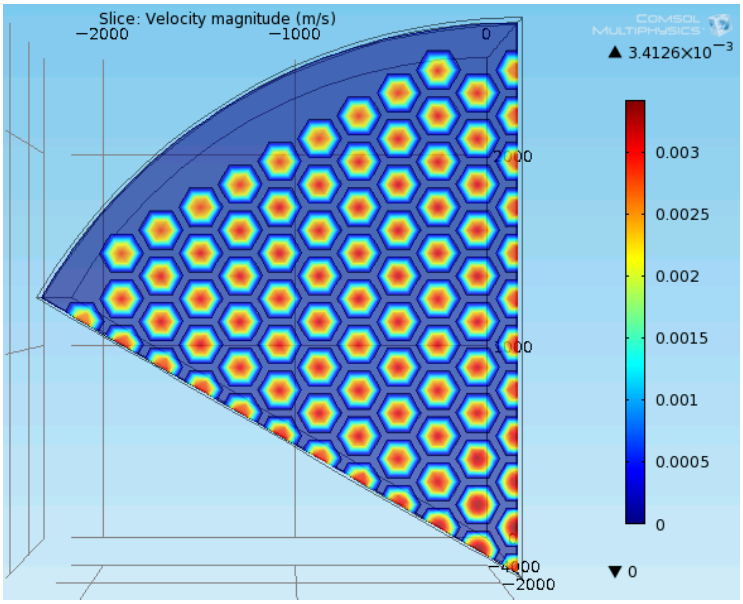

Supplementary Fig. 10 Results of simulation of flow velocities at the surface of pore array. The lateral coordinates (x, y) on the pore array surface are stated in µm (2000 µm = 2 mm), and the flow velocities (in z direction) are given, using the color scale, in meters sec^{-1} (0.003 m sec^{-1} = 3 mm/sec.). This flow profile gradually transforms into that of the laminar flow characteristic of the simple tube as the cross section is calculated for positions (z coordinates) above the pore array surface. The transition is nearly complete at z = 5 mm. Supplementary Figure 3 shows that the rapid spatial variations in fluid velocities across each pore extend only a few pore diameters (~ 0.1 mm) above the pore array surface.

To visualize magnetic capture and release phenomena we have used magnetically labeled, CellTracker stained H1650 cells at low densities and without whole blood. In this case, we followed the R&D Systems labeling protocol, which includes washing steps to remove un-reacted magnetic labeling antibodies and magnetic nanoparticles. For Supplementary Movie 3, we used a 10X objective with NA=0.2 which results in better lateral resolution, smaller pixel spacing and shallower depth of field. The gap between the magnetic sifter surface and the top window is 2 mm here, for which whole blood suspensions are unacceptably opaque, so that cells which are moving through the flow cell become heavily distorted when they are not in the focal plane. The nominal lateral velocities of cells are also reduced here, relative to the thin (0.1 mm) gap cell used for spiked samples, because of the larger gap. Supplementary Figure 11 shows an excerpted image of fluorescent cells, with pores partially revealed by tilted transmitted backlighting. The full movie shows cells in flow, both with and without the magnetizing field, and also demonstrates the release of captured cells when the field is removed soon after capture, and the flow is reversed and slightly increased.

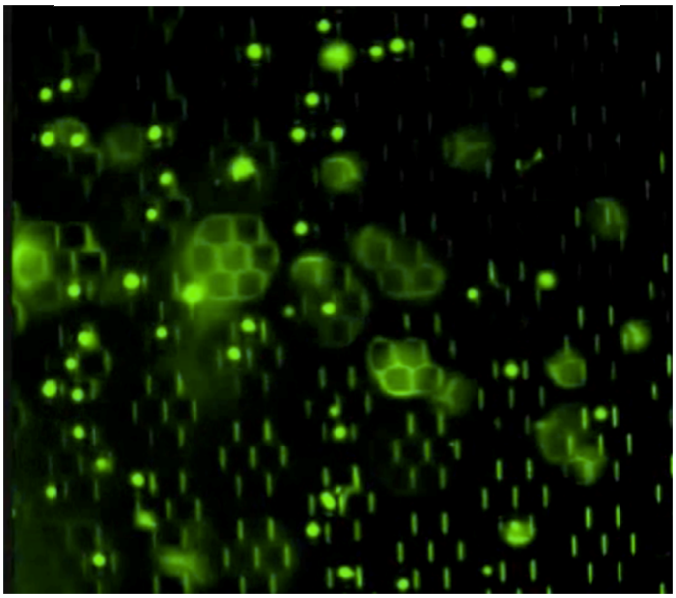

Supplementary Fig. 11 Live observation of capture behavior (excerpt image from Supplementary Movie 3). Supplementary Movie 3 shows H-1650 cells, pre-labeled with CellTracker Green, passing through the magnetic sifter in the absence of an applied magnetic field. When a field is applied, cells are captured at the edges of the pores. Upon removing the field and reversing the direction of flow, captured cells are released from the pore array. Pore edges are 50 μm.

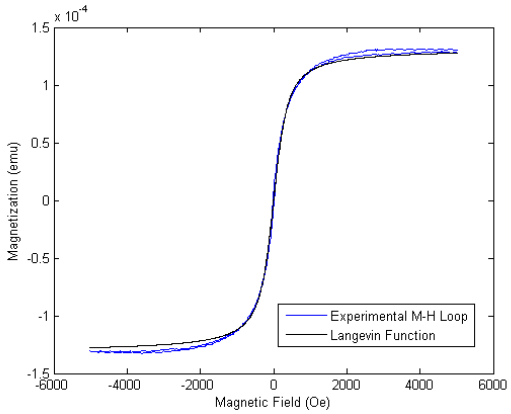

Supplementary Fig. 12 AGM result and Langevin function curves for H1650 cells after incubation with magnetic nanoparticles. The above M-H curve (blue curve) yields a saturation moment of 130 μemu for 9 x 10^5 cells after incubation with 0.1mg/ml of biotinylated Anti-EpCAM antibody (Clone 9C4, Biolegend) and 100ul of magnetic nanoparticle stock solution (MagCellect Streptavidin Ferrofluid, R&D Systems, Cat. #MAG999). This yields an approximate value of 1.4 x 10^{-10} emu per cell. The black curve is the magnetization obtained by using the Langevin function, and is the functional form used in Comsol.